


# Fluorine-Containing Bioactive Glass Spherical Particles Synthesized By Sol-Gel Route Assisted by Ultrasound Energy or Mechanical Mixing

Ingrid Elen Pinto e Souza<sup>a,\*</sup> , Sandhra Maria de Carvalho<sup>a</sup>, Talita Martins<sup>a</sup>,  
Marivalda de Magalhães Pereira<sup>a</sup>

<sup>a</sup>Universidade Federal de Minas Gerais, Escola de Engenharia, Departamento de Engenharia de Metalúrgica e de Materiais, Belo Horizonte, MG, Brasil.

Received: February 18, 2020; Revised: May 05, 2020; Accepted: June 07, 2020.

Bioactive glasses (BG) are versatile materials for various biomedical applications due to their capacity to bond to hard and soft tissues. These materials can be produced with different nominal compositions, such that include fluoride ions. Fluorine-containing-BG (BGF) can be produced by the sol-gel method, and its properties can be changed by altering the synthesis parameters. Here, BGF particle size between 235 nm-390 nm were obtained through sol-gel method assisted by ultrasound energy (BGU) or through mechanical stirring (BGM). The BGM and BGU particles showed highly dispersed spherical shape, moreover BGM are mesoporous and BGU are dense structures, indicating mixing mode can alter mainly the material textural characteristics. All compositions have apatite forming ability, verified by DRX from 14 days in SBF. The results showed  $\text{CaF}_2$  on the surface of BGF particles, indicating that part of F ions was not incorporated in the material network. The samples did not show any cytotoxicity towards human cells in Cellular Metabolic Activity and Calcein assays. This study showed that mechanical agitation was more efficient to produce mesoporous particles to be applied as carrier of drugs and molecules to the biological environment, so BGM can be used as a more efficient biomaterial for such applications.

**Keywords:** Bioactive glass, Fluorine, mechanical stirring, ultrasound energy, sol, gel.

## 1. Introduction

Bioactive glass (BG) is a synthetic bioceramic material developed by Larry Hench, which has high visibility in medicine for its ability to bond to bone via formation of an hydroxycarbonate apatite (HCA) layer on the material surface when in contact with the physiological environment<sup>1</sup>. This bonding to bone feature can be enhanced by adding different ions to the BG network, such as fluoride, which promotes the formation of fluorapatite (FA), a compound with improved chemical stability when compared to HCA<sup>2</sup>. Fluorine-containing bioactive glass (BGF) has been extensively studied for the treatment of dentine hypersensitivity, that causes patient acute pain in the nerve endings of the teeth, a condition that reaches about 35% of the world population<sup>1,3-6</sup>.

BGF are traditionally produced through melting routes, in which the precursor oxides are fused together with the F precursor, generally  $\text{CaF}_2$ <sup>7</sup>. However, in fusion routes there is some fluoride loss during melting, besides the fusion route can generate particles with a large size range, and irregular morphology, which can cause micro-cuts and micro-lesions at the implant site, thus limiting their applications<sup>8</sup>. An alternative to obtain BGF is the sol-gel route<sup>7</sup>.

The sol-gel process involves a sequence of hydrolysis and condensation reactions of silica precursor in aqueous solution at room temperature<sup>9</sup>. The final product is a porous material, with pores that can range in size from 20 to 700 nm, higher

surface area and greater porosity, that may have the spherical morphology and better dispersibility, when compared to the glasses produced by the fusion route. Those characteristics are influenced by the synthesis parameters, as the precursor concentration, the glass composition, the pH of the reaction, the temperature reaction, the rate of reagent addition, the surfactant choice and the reagents mixing methodology<sup>1,10</sup>. Furthermore, according to Jafarzadeh et al.<sup>11</sup>, the reagents mixing mode should be carefully defined as it could influence the reagents molecules active sites availability for further reactions. The BG and BGF production by the sol-gel method could provide improved material properties control, such as chemical composition, particle size, particle shape and pore structure<sup>12</sup>. These characteristics may allow the increase of the material dissolution rate in the biological environment and, as a result, stimulate the rapid formation of HCA layer at the tissue interface, so controlled synthesis is critical to the effective use of BG in biomedical applications<sup>13-15</sup>.

There are several researches in bioactive glass sol-gel process that investigates the difficulties in controlling the particle size, aggregation and agglomeration, therefore determining the properties of BG are highly related to the synthesis process<sup>12,16-19</sup>. Oliveira et al.<sup>16</sup> obtained spherical BG particles by the co-precipitation method in a diluted system using polyethylene glycol (PEG) as a dispersing agent that was assisted by ultrasonic catalysis, then, by this approach, it was possible to reduce the solvent use

\*e-mail: [ingrid-eps@ufmg.br](mailto:ingrid-eps@ufmg.br)

and the gelation time and to engineer BG particles with a well-defined morphology and narrow size distribution by adjusting the PEG chain length to modify the surface activity in the sol-gel reaction<sup>16</sup>. Zheng et al.<sup>18</sup> studied the influence of timing of calcium nitrate (calcium precursor) addition during processing on BG nanoparticles characteristics. The results showed that the addition timing could affect the morphology, dispersity and composition of BG nanoparticles, once delayed addition of calcium nitrate, larger, more regular and better dispersed BG nanoparticles could be synthesized, while the gap between nominal and actual compositions of BGN was widened<sup>18</sup>. Thus, the present work focuses on the evaluation of the synthesis parameter agitation mode, to produce spherical and submicrometric bioactive glass particles and fluorine-containing bioactive glass particles via a simplified sol-gel process. The influence of the reactants mixing mode (mechanical stirring and ultrasonic energy), which were not previously reported, was investigated. The effect of the reactants mixing mode on the structure of the obtained materials, the formation of apatite layer on their surfaces through bioactivity study and its biological properties in vitro were investigated.

## 2. Materials and Methods

### 2.1. Materials

The bioactive glasses were synthesized using the following reagents: tetraethyl orthosilicate (TEOS:  $C_8H_{20}O_4Si$ - 98% purity, Sigma-Aldrich, Saint Louis, USA), triethyl phosphate (TEP:  $C_6H_{15}O_4P$ - Sigma- Aldrich, Saint Louis, USA), tetrahydrate calcium nitrate ( $Ca(NO_3)_2 \cdot 4H_2O$  - 99% purity-Synth) and calcium fluoride ( $CaF_2$  - 96% purity, Vetec), ethyl alcohol (EtOH:  $C_2H_6O$ - 95% purity, Synth), ammonium hydroxide solution ( $NH_4OH$ - 27% content, Synth) and cetyl trimethylammonium bromide (CTAB:  $C_{19}H_{42}BrN$ - 99% purity, Vetec) was used as templating agent. All reagents used were of analytical grade, and Milli-Q water was used in all solutions (18.0 M $\Omega$ ·cm).

### 2.2. Methods

#### 2.2.1. Bioactive glass particles synthesis

Bioactive glass submicron particles (BG) were prepared by a sol-gel route as described by Hu et al.<sup>14</sup> in a prior study, with two different nominal compositions in mol. BGM and BGM reagents were mixed by mechanical stirring (280 rpm), and BGU and BGFU reagents were mixed by ultrasonic

stirring -Hielscher- Ultrasound Technology, model UP200S (220V, 24kHz)- with 60% amplitude and 0.6 frequency, producing 4 different samples, as described in Table 1. First, 0.407 g of CTAB was dissolved in 165 mL of deionized water (DW) and 78 mL of absolute ethanol (EtOH) under stirring during 30 min. Next, 3 mL of ammonium solution, 3 mL of tetraethyl orthosilicate (TEOS), 0.23 mL triethyl phosphate (TEP), 0.64 g of  $Ca(NO_3)_2$  were added to the solutions with 30 min interval between each reagent addition. To produce fluorine-containing bioactive glass, 0.148 g of  $CaF_2$  and 0.195 g of  $Ca(NO_3)_2$  were added. The sol was stirred for another 3 h at room temperature. The white precipitate produced was collected by filtration in filter paper Millipore 0.22  $\mu m$ , rinsed with EtOH and DW and dried at room temperature for 24 h. The bioactive glass particles were obtained after thermal treatment. The samples were placed in crucible and heated at a rate of 2  $^{\circ}C/min$  up to the 650  $^{\circ}C$  in a furnace, then held for 3 h, and cooled to room temperature inside it<sup>14</sup>.

#### 2.2.2 Chemical composition analysis

The chemical compositions were analyzed by inductively coupled plasma optical emission spectroscopy (ICP-OES). PerkinElmer Optima 7300 DV ICP-OES equipment was used to determine the Si, Ca and P concentrations. A total of 0.1 g of each sample was transferred to a graphite crucible containing 0.7 g of anhydrous lithium metaborate. Then, another 0.7 g of anhydrous lithium metaborate was transferred to the graphite crucible and fused at 950  $^{\circ}C$  for 10 min. The crucible was removed from the furnace, and the mixture was homogenized; then, it was fused another 10 min at 950  $^{\circ}C$ . After that, it was transferred to a beaker containing 100 mL of 10%  $HNO_3$  solution and stirred for 20 min. The concentrations of Si, Ca and P were then analyzed by ICP-OES, and the proportions of  $SiO_2$ , CaO and  $P_2O_5$  were calculated.

#### 2.2.3 Scanning electron microscopy (SEM) and Transmission electron microscopy (TEM)

Morphologies of the materials were observed by FEI-INSPECT S50 Scanning Electron Microscope (SEM), operating at the voltage of 15 kV, and by Tecnai G2-12 - SpiritBiotwin FEI - 120Kv Transmission Electron Microscope (TEM). The SEM equipment is equipped with Energy Dispersive X-ray Spectroscopy (EDS). Prior to examination by SEM, the samples were previously coated with graphite film by sputtering, to make them conductive. The EDS spectra were all obtained at the same accelerating

**Table 1.** Nominal composition and compositional analysis (mol%) of the bioactive glasses stabilized, determined by lithium metaborate fusion and ICP.

Samples	Stirring Method	Nominal composition (mol%)				Measured composition (mol%)			
		$SiO_2$	CaO	$P_2O_5$	$CaF_2$	$SiO_2$	CaO	$P_2O_5$	$CaF_2$
BGM	Mechanical stirring	80.0	15.0	5.0	-	88.8	11.1	0.1	-
BGU	Ultrasound-assisted	80.0	15.0	5.0	-	85.0	15.0	0.0	-
BGMF	Mechanical stirring	80.0	5.0	4.0	11.0	82.6	17.2	0.2	-
BGFU	Ultrasound-assisted	80.0	5.0	4.0	11.0	80.0	20.0	0.0	-

voltage of 12 kV. For TEM examination, the samples were dispersed in ethanol in a proportion of  $0.1 \text{ mg}\cdot\text{mL}^{-1}$ , mixed in an ultrasound bath for 30 min, and then collected on 400 mesh carbon coated copper TEM grids.

#### 2.2.4 Atomic Force Microscopy (AFM)

The Atomic Force Microscopy (AFM) analysis was performed to obtain a topographic image of the samples. This study used the AFM equipment- Park Systems XE-model- 70, leading type Si PPP-NCHR, in noncontact mode, with a constant force of 42 N/m and 330 kHz frequency. Sample preparation was performed by adding the powder of samples, after heat-treatment, in ethanol, at the concentration of  $1 \text{ mg}\cdot\text{mL}^{-1}$ , kept stirring for 5 h, and immediately after a droplet was dispensed on a coverslip for analysis.

#### 2.2.5 Dynamic Light Scattering (DLS)

The Dynamic Light Scattering analysis (DLS; Zetasizer 3000 HS 1256) was performed to measure the hydrodynamic diameter of the submicron particles after heat treatment. The system is equipped with a 4 mW He/Ne laser at 633 nm wavelength and measures the particle size at a detection angle of  $173^\circ$ . Light scattering measurements were made at  $25 \pm 1^\circ\text{C}$ . Hydrodynamic measurements were performed at a  $90^\circ$  angle. The data were analyzed according to the cumulative method to determine the apparent mean diameter and Polydispersity Index (PDI); the final value was a mean of 10 measurements. To evaluate the particle size, the samples were prepared from the glass dispersion in methanol at the concentration of  $0.01 \text{ g}\cdot\text{mL}^{-1}$ .

#### 2.2.6 Fourier transform infrared (FTIR) spectroscopy

The structure of the samples was analyzed by Fourier Transform Infrared Spectroscopy (FTIR), PerkinElmer 100 Spectrum. The spectra were collected in the mid-infrared range from 400 to  $4000 \text{ cm}^{-1}$  in reflectance mode. Samples were prepared by mixing and crushing the powder with potassium bromide (KBr, infrared grade) at a concentration of 1% (w/w). The FTIR spectra were reported after background subtraction and baseline correction, in the range of  $450\text{--}2000 \text{ cm}^{-1}$ .

#### 2.2.7 X-ray Diffraction (XRD)

X-ray diffraction (XRD) was performed on the samples thermally treated at  $650^\circ\text{C}$  to evaluate the crystallization and network modifier incorporation. XRD spectra of the particles were collected on a Philips PW1700 series automated powder diffraction analyzer, using Cu-K $\alpha$  radiation at 40 kV/40 mA. Data were collected between  $4^\circ$  and  $90^\circ$  with a step of  $0.02^\circ$  and a dwell time of 1 s.

#### 2.2.8 Nitrogen adsorption

The  $\text{N}_2$  adsorption-desorption isotherms were collected on a Quantachrome NOVA 2200 version 6.11, at 77 K. The specific surface area (SA) was determined by the Brunauer-Emmett-Teller (BET) method using adsorption data points in the relative pressure ( $P/P_0$ ) range of 0.01–0.30. The pore diameter distribution was calculated using the Barrett-Joyner-Halenda (BJH) method applied to the desorption curves.

#### 2.2.9 Preliminary in vitro bioactivity study- SBF assay

The bone-bonding ability of a material is often evaluated by examining the ability of apatite to form on its surface in a simulated body fluid (SBF). For the in vitro bioactivity studies, the SBF was prepared according to Kokubo's protocol<sup>20</sup>. The formation of an apatite/HCA layer on the particles was evaluated after immersion in SBF solution at time periods of 12 h, 24 h, 5 d, 14 d and 28 d, at a weight to solution volume ratio of  $0.1 \text{ mg}\cdot\text{mL}^{-1}$ . The surface structural observation was carried out after the immersed samples were removed from the SBF, washed three times with deionized water, and dried in an air circulation drying oven. To examine the newly formed HCA layer on the surface of the particles, the samples were analyzed by SEM, FTIR and XRD.

#### 2.2.10 Cytotoxicity evaluations

##### 2.2.10.1 Cell culture

In this study, embryonic kidney cells (HEK 293 T) were cultured in DMEM (Dulbecco's modified eagle medium) with 10% FBS (fetal bovine serum), streptomycin sulfate ( $10 \text{ mg}\cdot\text{mL}^{-1}$ ), penicillin G sodium ( $10 \text{ units}\cdot\text{mL}^{-1}$ ) and amphotericin-b ( $0.025 \text{ mg}\cdot\text{mL}^{-1}$ ), all from Gibco BRL (NY, USA), in a humidified atmosphere of 5%  $\text{CO}_2$  at  $37^\circ\text{C}$ .

The 'in vitro' tests were conducted according to ISO standards 10993-5:1999 (Biological evaluation of medical devices; Part 5: tests for in vitro cytotoxicity). For all *in vitro* tests, the raw materials were sterilized by UV radiation for 60 min.

##### 2.2.10.2 Cellular metabolic activity

HEK293 T cells on passage 35 were plated ( $1 \times 10^4$  cells/well) in 96-well plates for 24 h without FBS for synchronization. After that, the medium was aspirated, replaced with DMEM medium with 10% FBS, and the BGM, BGU, BGFm and BGFu samples were added ( $1 \text{ mg}\cdot\text{mL}^{-1}$  (w/v)). Control references were created using cells and DMEM with 10% FBS, Triton x-100 (1% v/v PBS; Sigma-Aldrich, St. Louis, MO, USA) as a positive control, and chips of sterile polypropylene ( $1 \text{ mg}\cdot\text{mL}^{-1}$ ; Eppendorf, Hamburg, Germany) as a negative control. After 48 h incubation, the medium was replaced with 60  $\mu\text{L}$  of culture medium with 40  $\mu\text{L}$  of MTT ( $5 \text{ mg}\cdot\text{mL}^{-1}$ , Sigma-Aldrich, St. Louis, MO, USA) and the plates incubated for 4 h at  $37^\circ\text{C}$  and 5%  $\text{CO}_2$ . After that, 40  $\mu\text{L}$  of isopropanol 4% HCl 0.04 N solution was added. Subsequently, 100  $\mu\text{L}$  was removed from each well and transferred to a 96-well plate, where absorbance was quantified at 595 nm using a spectrometric microplate reader (I-Mark, Bio-Rad). The obtained values were expressed as the percentage of viable cells. All data were analyzed using Prism software (Software GraphPad, San Diego, CA, EUA) and the results were expressed as the average  $\pm$  standard deviation for 6 replicates ( $n = 6$ ). Statistical significance was determined for all groups using a one-way ANOVA/Bonferroni test considering  $p < 0.05$  to be statistically significant.

##### 2.2.10.3 Calcein assay

For this assay, the cells were plated in the same manner as in the MTT assay. After 48 h, the medium was removed, the cells were rinsed 3 times with PBS (Gibco BRL, New York,



EUA) and their viability was assessed by Calcein AM (Life Technologies do Brazil Ltd., São Paulo, Brazil) according to the manufacturer's protocol. Cells were analyzed by an inverted optical microscope (Leica DMIL LED, Germany) and the fluorescence emissions of Calcein were collected at  $530 \pm 12.5$  nm.

### 3. Results and Discussion

#### 3.1 Chemical composition

The glasses chemical composition (mol%) were analyzed by the lithium metaborate fusion method and ICP-OES analysis. The results are shown in Table 1 but it does not show  $\text{CaF}_2$  compositions, since the technique is not sensitive to fluorine capitation.

Differences between the glass nominal composition and the ICP-OES composition were observed, mainly with respect to the presence of phosphorus pentoxide ( $\text{P}_2\text{O}_5$ ). The phosphorus precursor (TEP) was added in much smaller quantities compared to the other reagents and it is a compound that reacts slower than TEOS (Si precursor). This fact may have affected phosphorus insertion in the silica network, which would account for the smallest fractions of phosphorus ( $\text{P}_2\text{O}_5$ ) in the synthesized glasses<sup>21</sup>. The amount of calcium incorporated in the resulting gels depends on the initial composition. During polycondensation calcium ions may be adsorbed or incorporated in the gel network, but it

is likely that part of the ions remains in the solution. Some calcium ions may also be leached out during the particles washing stage with water and ethanol. These two reasons may account for the lowest proportion of calcium present in the particles, as determined by the ICP analysis of BGM and BGU<sup>16</sup>. For glasses containing fluoride ions, the particles have lower Silica content and the final calcium percentage is higher. Other techniques are necessary to evaluate how Ca is present in the particles produced.

#### 3.2 Morphological analysis

Figure 1 shows SEM micrographs of BGM, BGU, BGMF and BGFU. It was possible to observe that all samples showed a predominant monodispersed spherical morphology.

The spherical shape of the samples was confirmed by AFM (Figure 2) and by TEM (Figure 3). By TEM it was also observed the presence of pores in the BGM and BGMF particles.

The sphericity of bioactive glass particles is an important feature for dental applications, such as in the treatment of dentin hypersensitivity, since the irregular morphology could cause micro-cuts and micro-injuries at the implant site, increasing the healing time<sup>2,8,14</sup>. Moreover, the cell adhesion and proliferation in materials with spherical morphology are greater when compared to materials with irregular morphology since there will not be a physical barrier to prevent their movement<sup>22</sup>.

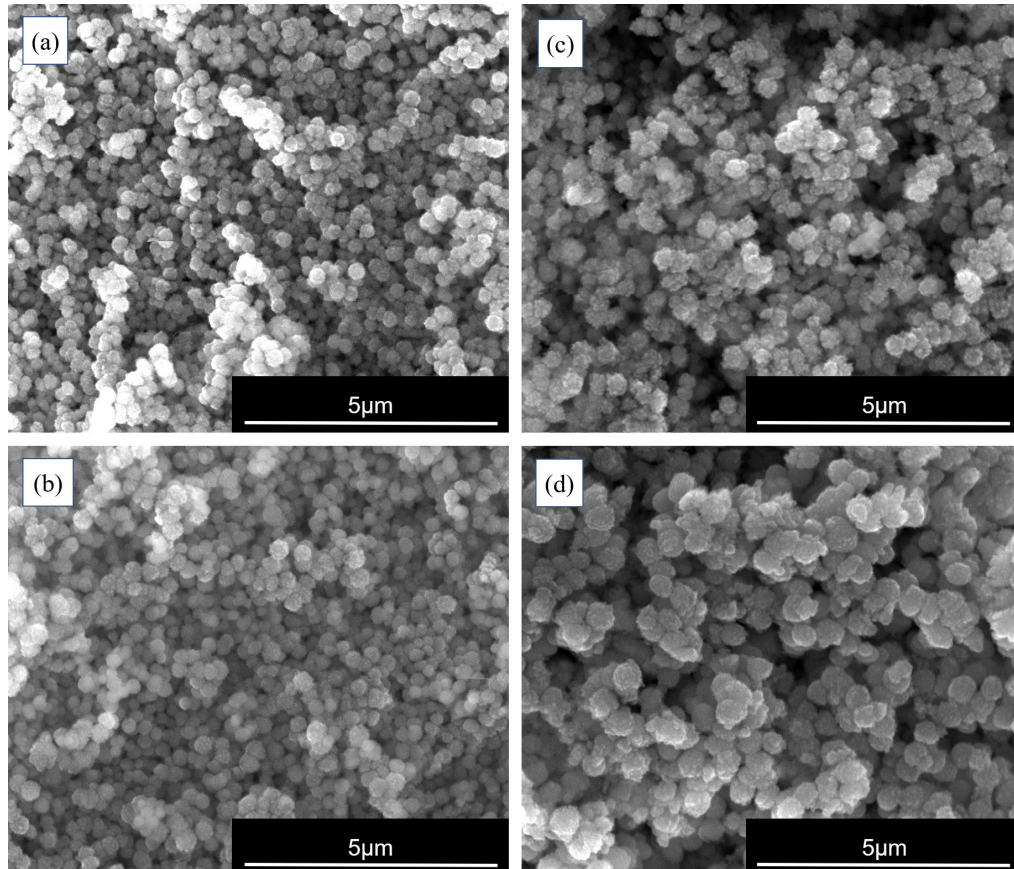


**Figure 1.** SEM micrographs images of (a) BGM; (b) BGU; (c) BGMF; and (d) BGFU spheres.



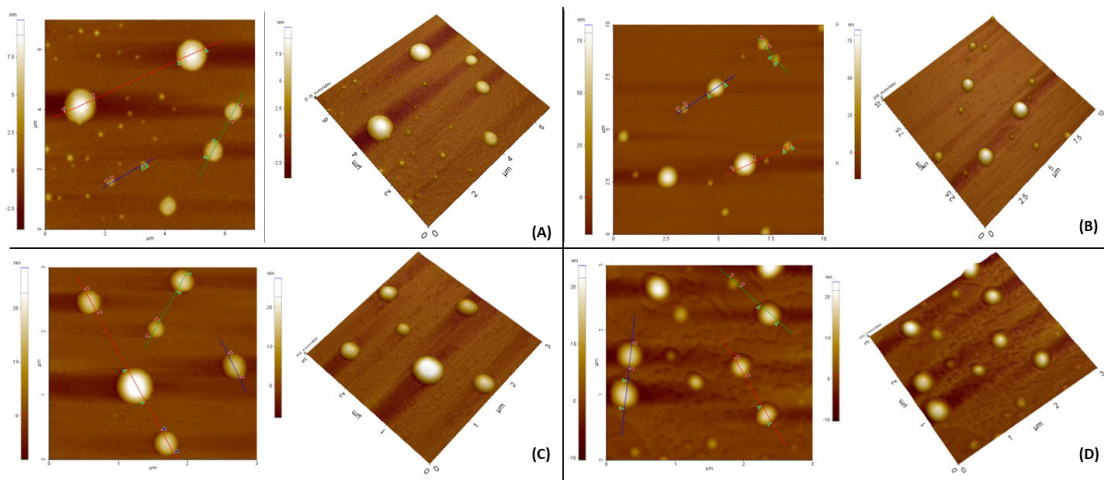


**Figure 2.** AFM image of (a) BGM; (b) BGU; (c) BGFM; and (d) BGFU and their respective particle size analysis.

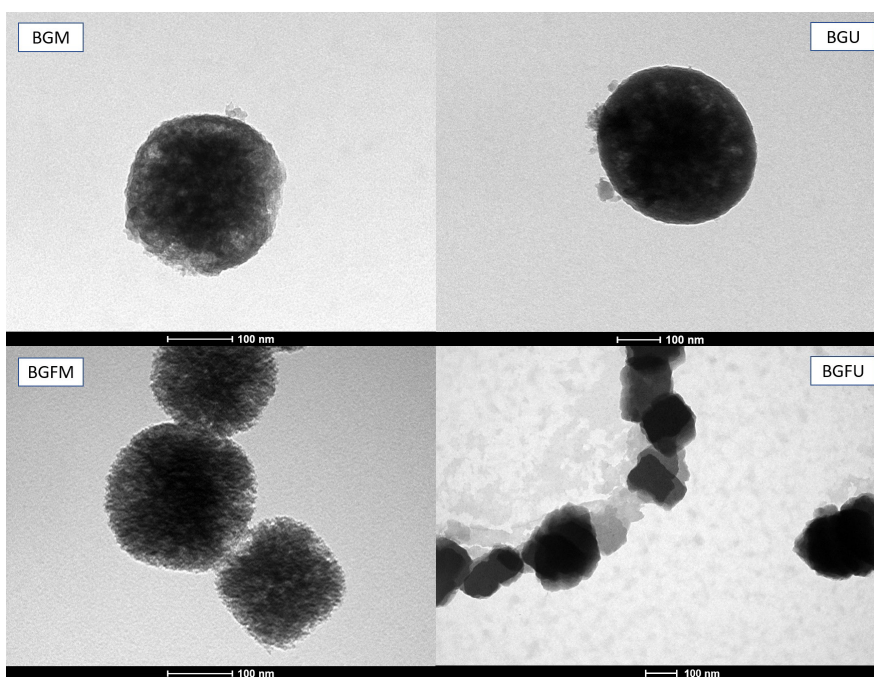


**Figure 3.** MET image of (a) BGM; (b) BGU; (c) BGFM; and (d) BGFU.

The particle size distribution in suspension was obtained by DLS analysis (Table 2). The cumulative analysis obtained by DLS showed an average particle diameter greater than 100 nm, which is characterized as submicrometer sized<sup>1</sup>. The Polydispersity Index (PDI) indicated values around 0.3 for all samples. The results of PDI suggest that each sample had a homogeneous distribution of particle sizes<sup>23</sup>. Hu et al.<sup>14</sup> obtained an average particle size of 264 nm for a similar processes of BGM sample synthesized here. Ghadiri et al.<sup>24</sup> produced sub-micron BG particles, by a similar sol-gel route using CTAB as a surfactant, with average particle size of 250 nm. Therefore, the range of particle size distribution values obtained here are in line with the values found in the literature for similar sol-gel routes. The particle size ranges of BGM ( $197 \pm 23$  nm) and BGFM

**Table 2.** Particle size obtained by DLS analysis.

	DLS (nm)	PDI
BGM	$196.8 \pm 22.5$	0.30
BGU	$233.9 \pm 20.0$	0.22
BGFM	$389.7 \pm 41.0$	0.35
BGFU	$234.7 \pm 22.5$	0.28

PDI = polydispersity index

( $390 \pm 4$  nm) are not similar, while the particle size ranges of BGU ( $234 \pm 20$  nm) and BGFU ( $235 \pm 23$  nm) present low variation. Apparently, the addition of  $\text{CaF}_2$  influenced the particle size of glasses synthesized via mechanical stirring, but it did not influence the particle size of glasses synthesized via ultrasound energy. Therefore, to explain the influence of

the addition of  $\text{CaF}_2$  on particle size is not straightforward, and a more detailed knowledge of the amount of Ca and F in the glass network would be necessary. Possibly the differences in particle size ranges occurred due to different synthesis conditions provided by the two different methods of mechanical stirring and ultrasonic energy, such as the variation of synthesis temperature. In this work, the initial and the final synthesis temperatures were checked. Under mechanical stirring, the suspension temperature remained constant at 25 °C. Using the ultrasound energy, there was an increase in temperature, since the initial temperature was 25 °C and the final temperature was 50 °C. The principle of ultrasonic energy, the sonocavitation, create gas bubbles and increases the medium temperature, acting as nanoreactors, where the synthesis happens faster<sup>16</sup>. A study of mixing methodology in the synthesis of silica particles performed by Rahman et al.<sup>25</sup> analysed suspensions with initial synthesis temperature of 25 °C, by mechanical stirring and ultrasonic energy. The final temperature of the suspension under ultrasonic energy had an increase to 52 °C, and a decrease in the particle size was observed. The small particle size produced assisted by ultrasound energy can be explained by an increase in the silica nucleation rate due to the increase in temperature<sup>25</sup>. However, in the present work it was not possible to observe consistent differences in the particle sizes found, to allow an analysis of the effect of either composition or mixing method used.

### 3.3 Structural analyses

The structural analysis of BG and fluorine-containing BG sub-micrometrical particles was performed by FTIR after heat treatment. FTIR spectra presented typical bioactive glass absorption bands, as showed in Figure 4 and summarized in Table 3. The centered band at 467  $\text{cm}^{-1}$  can be attributed to the Si–O–Si bending vibration and is often related to amorphous glass structures. The symmetric stretching vibration of Si–O groups can be observed in the region of 800  $\text{cm}^{-1}$  and the centered band at 965  $\text{cm}^{-1}$  is related to Si-OH groups, whereas the asymmetric stretching of Si–O–Si groups are related to the band at 1090  $\text{cm}^{-1}$ . The P–O bending of  $\text{PO}_4^{3-}$  groups is assigned to the absorption at 560  $\text{cm}^{-1}$ . The stretching of P–O bonds can be observed at approximately 1160  $\text{cm}^{-1}$ , overlapping the band at 1200  $\text{cm}^{-1}$  related to the transverse vibration mode of Si atoms in cyclic species of bioactive glass. The broad band observed between 1630–1450  $\text{cm}^{-1}$  can be related to absorbed carbonate groups, whereas the band at 1500–1600  $\text{cm}^{-1}$  is assigned to absorbed molecular water on the glass surface<sup>16,21</sup>. No major differences were observed in the FTIR spectra of BGF when compared to the typical BG glass spectra<sup>26</sup>. Furthermore, no differences

can be identified in the FTIR spectra related to the synthesis mixing methodology.

The XRD patterns obtained for BGM, BGU, BGMF and BGMF are shown in Figure 5. The wide halo observed between 20° and 40° (2 $\theta$ ) confirmed the amorphous nature of the glasses. The amorphous condition is important for a controlled rate of ion release from the glass network, allowing the material bioactivity modulation<sup>27</sup>. In Fluorine-containing glasses (BGMF and BGMFU), it is possible to visualize crystalline peaks at 2 $\theta$  near 28°, 47°, 55°, and 87°, characteristic of calcium fluoride ( $\text{CaF}_2$ ) (JCPDS 88-2301). Although it is not known its quantity in the samples synthesized, the appearance of these peaks showing the presence of the  $\text{CaF}_2$  phase on the particles indicates that possibly the added salt did not

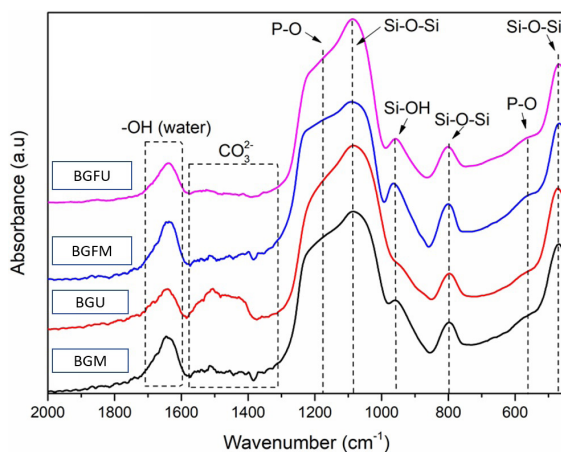


**Figure 4.** FTIR spectra of BGM, BGU, BGMF and BGMFU samples.

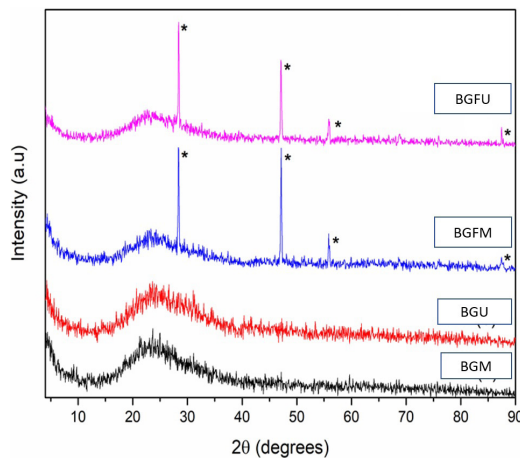


**Figure 5.** XRD patterns of (a) BGM; (b) BGU; (c) BGMF; and (d) BGMFU samples.

**Table 3.** Major FTIR vibrational bands associated with bioactive glass.

$\nu$ ( $\text{cm}^{-1}$ )	Assignment	References
1090	Si-O-Si (symmetric stretching)	Oliveira et al. <sup>16</sup> ; Barrioni et al. <sup>21</sup>
965	Si-O (bond stretching)	Oliveira et al. <sup>16</sup> ; Barrioni et al. <sup>21</sup>
800	Si-O-Si (symmetric stretching)	Oliveira et al. <sup>16</sup> ; Barrioni et al. <sup>21</sup>
467	Si-O-Si (bending)	Oliveira et al. <sup>16</sup> ; Barrioni et al. <sup>21</sup>
1160	P-O (stretching)	Oliveira et al. <sup>16</sup> ; Barrioni et al. <sup>21</sup>
560	P-O (bending)	Oliveira et al. <sup>16</sup> ; Barrioni et al. <sup>21</sup>

entirely solubilize, or that it may have reprecipitated during synthesis, and that the fluoride added may not have been incorporated into BGM and BGFU samples structure. This does not, however, exclude the possibility that at least part of the Fluoride ion has been incorporated in the glass structure. The presence of fluoride ions in BGs structure has been described by the formation of hypothetical “CaF<sup>+</sup>” species, in which Fluorine does not directly bond with silicon, but fluoride ions would be incorporated by the coordination of fluoride ions (F<sup>-</sup>) with calcium ions (Ca<sup>2+</sup>). Therefore the ionic group Ca<sup>2+</sup>F<sup>-</sup> (or CaF<sup>+</sup>) may form nano-agglomerates in the particles<sup>4,28,29</sup>. Even if CaF<sup>+</sup> ions were not incorporated in the glass structure, CaF<sub>2</sub> on the particles can act as a Fluorine carrier to the biological environment. Thereby, further studies should be conducted to confirm the presence of F in the glass network, such as the F release profile, using fluoride-selective electrode to analyze this ion in solution. Also, the use of specific techniques such as X-ray Excited Photoelectron Spectrometry (XPS) and Nuclear Magnetic Resonance Spectroscopy (NMR spectroscopy), would allow elemental composition, the chemical and the electronic state of the elements present, and, therefore, to better understand how the F ion enters in the glass network. No major differences were observed in the BG XRD patterns when comparing the two mixing modes used.

### 3.4 Textural characteristics

Figure 6 shows the adsorption-desorption isotherms and the pore distribution profile (inserted graph) obtained through the Nitrogen sorption analyzes. The adsorption-desorption isotherms of all samples were identified as type IV, which is characteristic of mesoporous material. Mesoporosity (2-50 nm)

is a typical feature of materials synthesized in the presence of CTAB<sup>12</sup>. The importance given to materials in this range of porosity is due to the faster induction, nucleation and crystallization, and greater amount of carbonated hydroxyapatite (HCA) layer formed in physiological medium, since they have high surface area<sup>30-32</sup>. The isotherms exhibited type H1 hysteresis loops, indicating pores with the shape of cylindrical channels<sup>32,33</sup>. However, the hysteresis loops of BGU and BGFU are smaller than BGM and BGFU, indicating that BGU and BGFU are materials with few interconnected pores, and a bulk denser than the materials surface<sup>34</sup>. This can also be seen in the TEM image (Figure 3), where BGs synthesized through ultrasound energy appears less porous than BG synthesized through mechanical stirring. According to Lins et al. (2017) sonogels in general presents characteristics of higher density structure, which explain denser particles produced by ultrasound energy when compared with that produced by mechanical mixing.

Table 4 data shows BGs and Fluorine-containing BGs surface area, total pore volume and pore diameter. The glass surface area produced by the same stirring method

**Table 4.** Characterization summary obtained from nitrogen sorption isotherms of bioactive glasses.

Samples	Surface Area (m <sup>2</sup> /g)	Total Pore Volume (cm <sup>3</sup> /g)	Average Pore Diameter (nm)
<b>BGM</b>	486.8	0.615	5.0
<b>BGU</b>	550.7	0.382	2.8
<b>BGFM</b>	612.7	0.492	3.2
<b>BGFU</b>	684.2	0.462	2.7

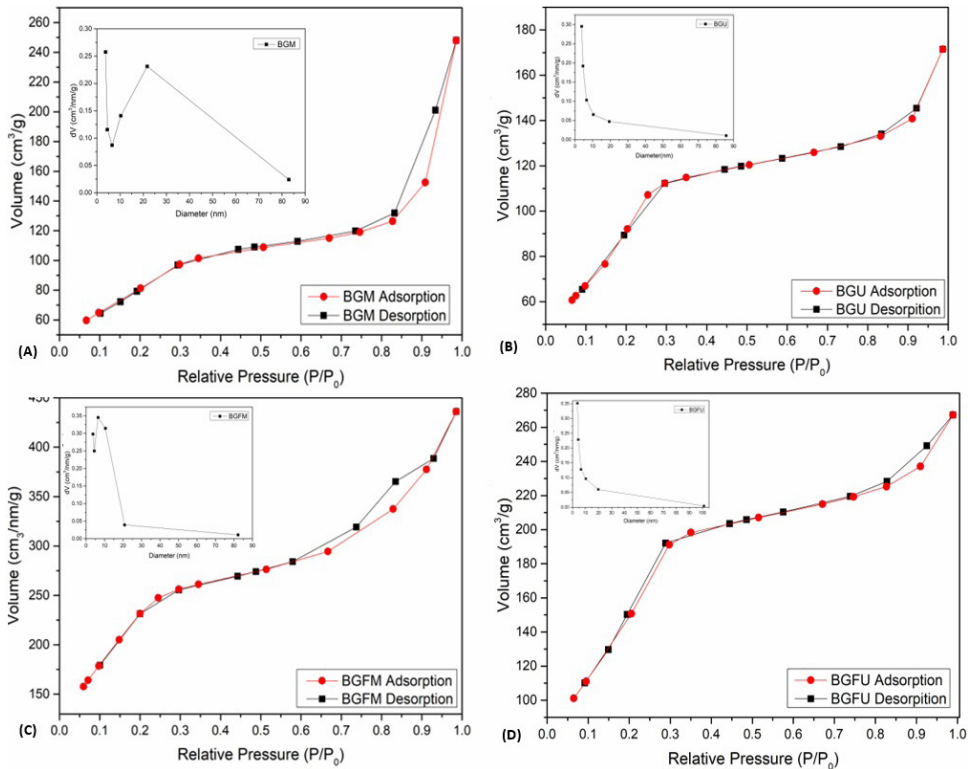


**Figure 6.** N<sub>2</sub> sorption isotherms and pore size distributions of a BGM, BGU, BGFU and BGFU.



(BGM and BGMF; BGU and BGFU) showed an increase with the addition of Fluoride ions. It was also observed that the surface areas of the glasses synthesized by ultrasonic energy (BGU and BGFU; 551 m<sup>2</sup>/g and 684 m<sup>2</sup>/g, respectively) were larger than the obtained for the glasses synthesized by mechanical stirring (BGM and BGMF, 487 m<sup>2</sup>/g and 613 m<sup>2</sup>/g, respectively), regardless of the Fluoride ions addition. Therefore, it is possible to affirm that BGFs had a surface area approximately 1.25 times greater when compared with BGs, for the same mixing method, and that texture of bioactive glass is dependent of mixing method and the presence of Fluoride ions in its synthesis. The incorporation of additional ions, such as fluorine ions, into the BGs structure can affect the network orientation during the self-assembly reaction, consequently disrupting the BG network, leading to potential structural defects, and also to modification on the pore shape, which can explain the largest surface area of fluorine-containing bioactive glasses<sup>35,36</sup>. The results of surface area and pore size obtained in this work are in line with the results obtained by Hu et al.<sup>14</sup> and Wang et al.<sup>37</sup>. Hu et al.<sup>14</sup> obtained surface areas for their particles of 599.963 m<sup>2</sup>.g<sup>-1</sup> and pore size of 5.696 nm for the synthesis corresponding to BGM<sup>14</sup>. Wang et al.<sup>37</sup> obtained surface areas for their particles of 591.765 m<sup>2</sup>.g<sup>-1</sup> and pore size of 4.887 nm in a synthesis under basic conditions and using CTAB as surfactant<sup>37</sup>. Here, it was obtained surface areas values between 487 m<sup>2</sup>.g<sup>-1</sup> (BGM) and 684 m<sup>2</sup>.g<sup>-1</sup> (BGU), and pore size of 5.0 nm was found for BGM. This indicates that the values found here are in line with the values reported in the literature for similar synthesis<sup>14</sup>. The average pore size for BGU (2.8 nm), BGMF (3.2 nm) and BGFU (2.7 nm) samples were reduced in relation to BGM average pore size. As this work indicates, the reduction in average pore size could be altered due to the addition of fluorine ions in the

glass synthesis and by the agitation methodology employed in the sol-gel route.

### 3.5 Preliminary *in vitro* bioactivity study - SBF assay

The bonding ability of a material is often assessed by the evaluation of its ability to form apatite on their surface when in contact with simulated body fluid (SBF)<sup>20</sup>. In this work, bioactive glass samples were immersed in SBF at 37 °C for different periods of time to evaluate their formation of HCA and /or FA on the material surface.

Figure 7 shows SEM micrographs of the BGs after immersion in SBF at the intervals of 12 h, 24 h, 5 d, 14 d and 28 d in order to visualize from which period the material's bioactivity started. It is possible to observe that at 12 and 24 hours the samples surfaces were smoother and homogeneous, passing to a flattened surface on the fifth day of analysis (Figure 7 – 5 d). According to De Caluwé et al.<sup>38</sup>, this modification in aspect is related to phosphate formation on the material surface. Progressing to the 14 d and 28 d, roughness could be identified and it is a indicative of a phase precipitation on the bioactive glasses surface, such as apatite<sup>39</sup>. In EDS spectra (Figure 8) it was possible to identify a reduction of the silicon peak (Si) between the immersion times of 12h and 28 d and an increase on the phosphorus (P) and calcium (Ca) peaks intensity, suggesting the precipitation of a calcium phosphate layer on the glass surface, which can crystallize to form an HCA layer<sup>40</sup>. These changes correspond to the apatite nucleation mechanism, where (1) occur ion exchange between the solution and the glass surface leading to the release of Ca<sup>2+</sup> and PO<sub>4</sub><sup>2-</sup> ions from the glasses into the medium, (2) followed by the release of soluble silica from the glass, (3) the polycondensation of silanol groups and formation of a porous layer rich in silica, (4) an increase in the concentration of Ca<sup>2+</sup> and PO<sub>4</sub><sup>3-</sup> in the solution, (5) the

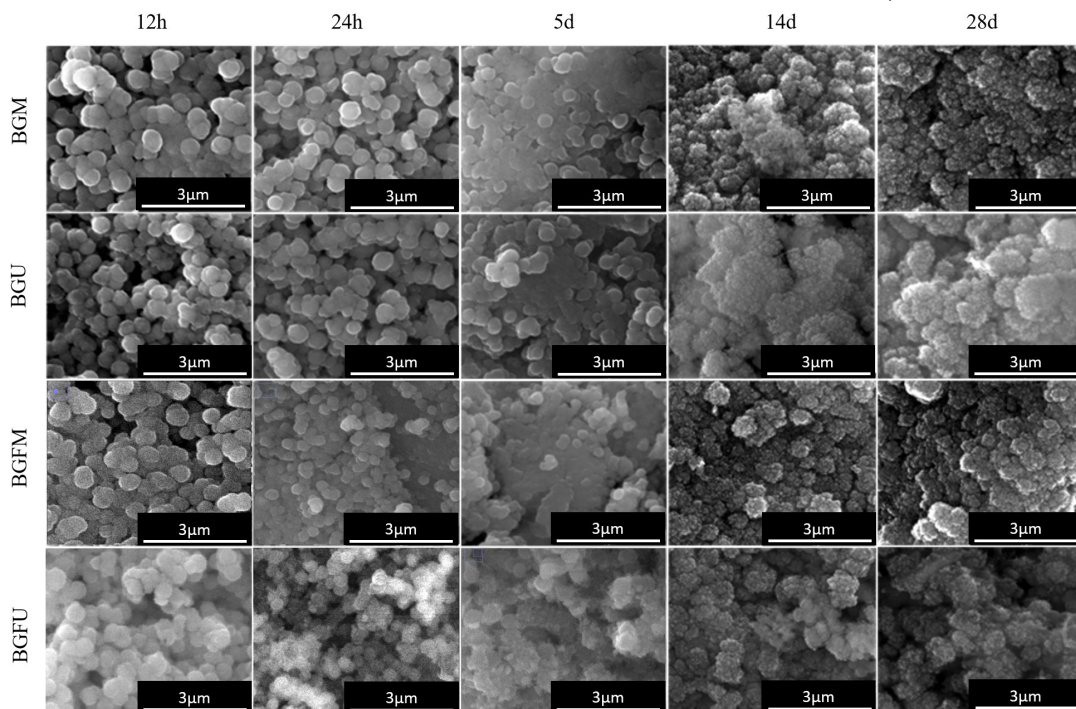


**Figure 7.** SEM micrographs of the surfaces of the BGM, BGU, BGMF and BGFU after incubation in SBF for 12 h, 24 h, 5 d, 14 d and 28 d.

formation of a film rich in amorphous calcium phosphate (ACP) and (6) the formation of a hydroxyapatite layer by incorporation of OH<sup>-</sup> and CO<sub>3</sub><sup>2-</sup> anions from the solution<sup>41</sup>. Fluorine was not identified by EDS due to the technique limitations, consequently, it was not possible to state through the EDS technique if the roughness presented is due to the FA formation in the Fluorine-containing BGs surfaces (BGM

and BGFU). From the 14th day it is possible to identify a peak related to sodium chloride (JCPDS 5-0628), that may have precipitated from the SBF solution, once this solution has a high concentration of Na<sup>+</sup> and Cl<sup>-</sup> ions.

The structure of the bioactive glasses after immersion in SBF was analyzed by FTIR (Figure 9). In general, no significant differences were identified between the sample's

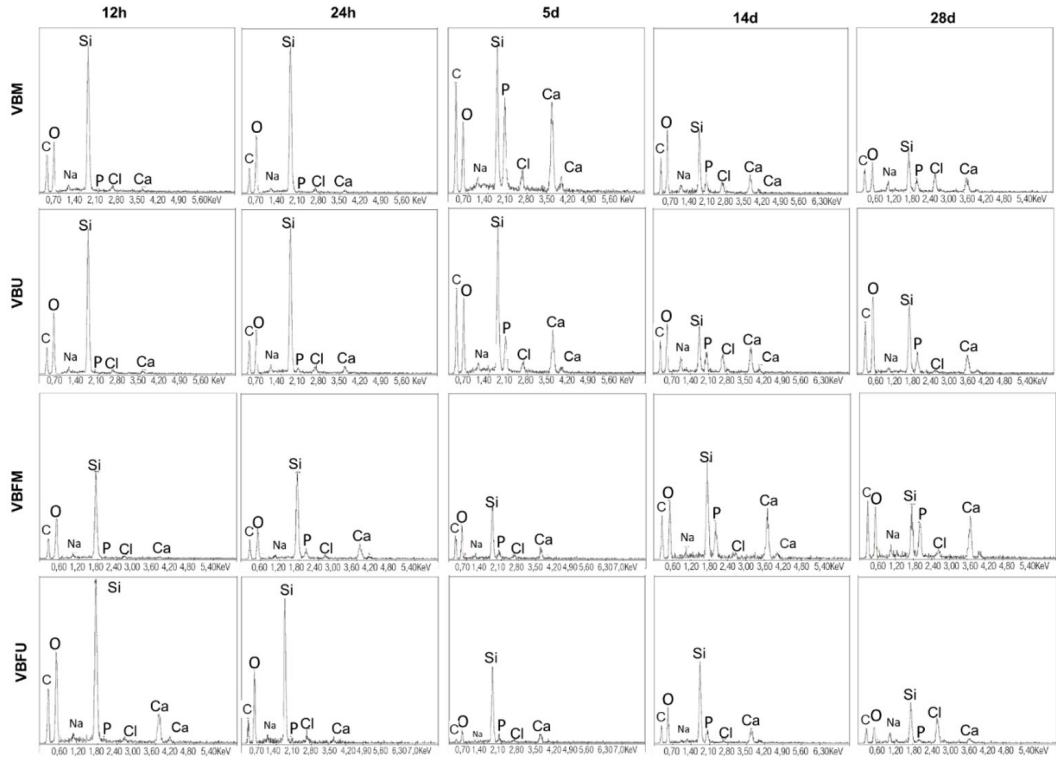


Figure 8. EDS spectra of the surfaces of the BGM, BGU, BGFm and BGFu after incubation in SBF for 12 h, 24 h, 5 d, 14 d and 28 d.

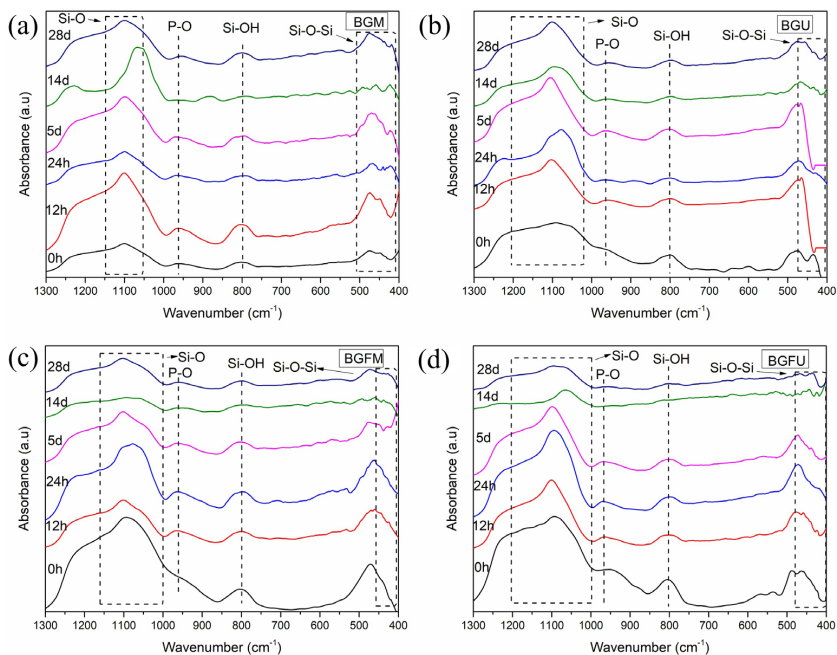


Figure 9. FTIR spectra of the surfaces of the (a) BGM, (b) BGU, (c) BGFm and (d) BGFu after incubation in SBF for 12 h, 24 h, 5 d, 14 d and 28 d.

spectra after immersion. The  $1100\text{ cm}^{-1}$  band is referred as the Si-O stretch band and can also be associated with the asymmetric P-O stretch ( $1050\text{ cm}^{-1}$ ), once the bands would be overlapping<sup>21</sup>. The band centered at  $960\text{ cm}^{-1}$  is associated to the symmetrical stretching of  $\text{PO}_4^{3-}$ , while the asymmetric stretching band of  $\text{PO}_4^{3-}$  is located at  $475\text{ cm}^{-1}$ <sup>121,26</sup>. The band centered at  $800\text{ cm}^{-1}$  is related to Si-O-Si vibrations in glasses before contact with SBF (0h), but after immersion in SBF the same band is associated with Si-O-Si and Si-OH groups formed by the ions exchange between the solution and the BG incorporated ions, which can indicate the formation of a silica gel layer on the BGs surfaces<sup>41,42</sup>. No major differences were observed in the FTIR spectra of fluorine-containing glasses when compared to the BG glass.

Figure 10 shows the XRD patterns of glass samples after immersion in SBF. The BGM and BGU samples showed an amorphous condition up to 5 days of immersion. From the 14th day, a crystalline peak can be identified for the BGU sample, which is associated to sodium chloride from the SBF solution. The XRD pattern of BGM and BGU samples shows peaks in  $2\theta$  at  $31^\circ$ , which is probably related to the carbonated apatite formation (JCPDS 19-272) and confirms the HAC formation on the samples surface after immersion in SBF<sup>43</sup>. After the immersion times of 12h, 24h, 5d and 14d the BGMF and the BGFU samples presented amorphous conditions, as shown by the halo at  $2\theta$  between  $15^\circ$  and  $35^\circ$ , and peaks of crystallinity related to calcium fluoride (JCPDS 35-816), possibly related to the precipitation of this salt in the fluorine-containing BG synthesis<sup>7</sup>. From the 5th day it is possible to identify a peak related to sodium chloride (JCPDS 5-0628), that may have precipitated from the SBF solution, once this solution has a high concentration

of  $\text{Na}^+$  and  $\text{Cl}^-$  ions. After 28 days of immersion, samples BGMF and BGFU presented peaks related to carbonated hydroxyapatite and / or fluorapatite (JCPDS 31-267), however the distinction of the two phases is hampered by the isomorphous property of these two minerals, so their peaks would be overlapping<sup>2,44</sup>. Al-Noaman and co-workers showed that  $\text{CaF}_2$  have an influence on bioactivity of the glasses, but are not incompatible with osteoblast-like cell viability because the cells were able to grow and proliferate on the glass surface, thus this implies that  $\text{CaF}_2$  enriched glass may be useful for stimulating osteoblastic growth and bone formation *in vivo*<sup>45</sup>.

Lusvardi et al.<sup>3</sup> showed that bioactive glasses containing Fluoride ions initiated the formation of HAC after 15 days of immersion in SBF, according to the exposed XRD patterns. However, pronounced peaks of the compound were only identified after 30 days of the solution immersion. Brauer et al.<sup>46</sup> studied the fluorine-containing glasses on immersion in SBF and verified HAC formation by intense peaks in XRD analysis after 14 days of immersion. However, the XRD patterns in this study showed broader bands, which would indicate that the crystals formed would be small and of highly disordered character. Brauer et al.<sup>46</sup> still found that glasses with high concentrations of fluorine ions tend to precipitate calcium fluoride on the surface of the particles, even after immersion in SBF. This would also happen because calcium fluoride is a compound of low water solubility. Other studies of *in vitro* bioactivity also showed, through the XRD patterns, the precipitation of  $\text{CaF}_2$  on the bioactive glass particles, such as those performed by Shah et al.<sup>40,47</sup>. These studies suggest that fluoride release from bioactive glasses often results in  $\text{CaF}_2$  formation and not FA or HCA. Therefore,

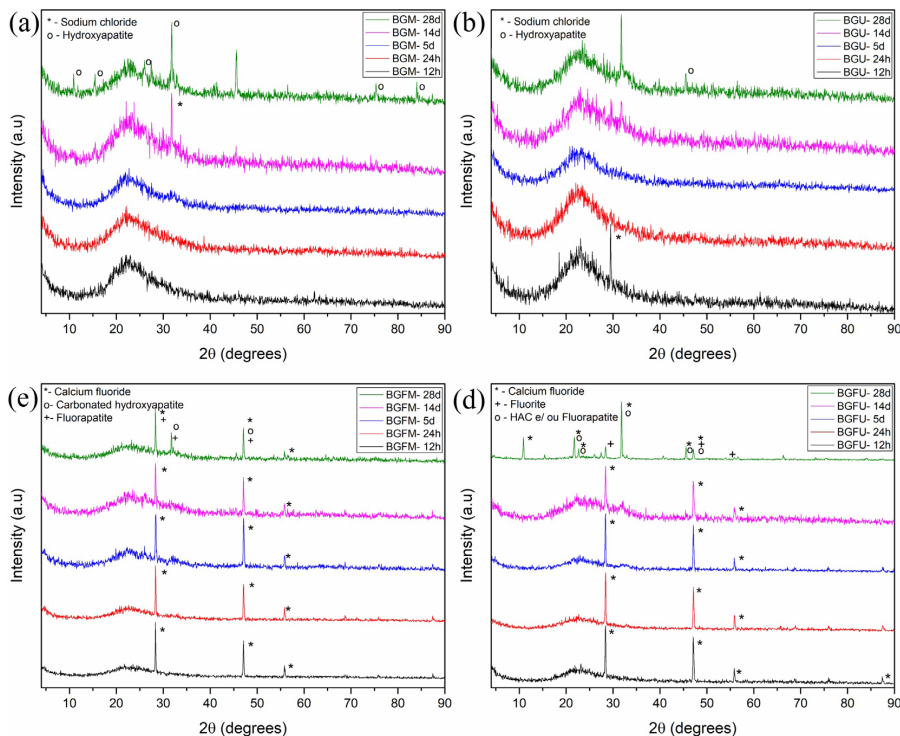


**Figure 10.** XRD patterns of the surfaces of the (a) BGM, (b) BGU, (c) BGMF and (d) BGFU after incubation in SBF for 12 h, 24 h, 5 d, 14 d and 28 d.



the results obtained in this work are in accordance with the results found in the literature.

In conclusion, the materials synthesized in this work started forming HCA at 14 d, and at 28 d of immersion in SBF the formation of HCA was clear. However, neither the synthesis agitation methodology nor the presence of fluoride ions in the glass composition altered significantly the bioactivity between the materials compared.

### 3.6 Cytotoxicity assay

The MTT ([3-(4,5-dimethylthiazol-2-yl)-2,5-diphenyltetrazolium bromide]) assay evaluates the presence of live and / or growing cells in biological medium. This assay consists of the ability of dehydrogenase enzymes, located in the mitochondria of viable cells, to convert the yellow soluble, water-soluble tetrazolium salt into formazan, a blue, water-insoluble salt. Thus, the amount of Formazan produced is proportional to the number of viable cells in the medium<sup>48</sup>.

The cytotoxicity assessment determined by MTT assay (Figure 11) showed that all the samples, both via mechanical stirring and via ultrasonic energy, had cellular viability varying between  $83.33 \pm 14.31\%$  (BGM) and  $101.50 \pm 11, 99\%$  (BGU). All the glasses were at levels

of viability above 70%, characterizing them as non-cytotoxic materials<sup>21</sup>. In this way, neither the method of agitation nor the addition of Fluoride ions to the glass interfered in the mitochondrial metabolic activity of the cells.

In this work the Calcein assay was used to qualitatively validate the results of the MTT assay. The Calcein assay was used for analysis of cytoplasmic function and cell membrane integrity<sup>49,50</sup>. HEK293 T cells were analyzed in contact with the samples after 48 h. All the samples showed similar fluorescence to the control group, i.e. high green fluorescence (viable cells) (Figure 12). It can be concluded

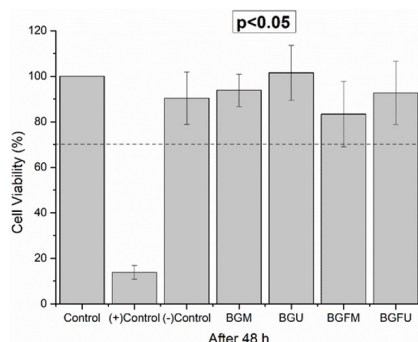


Figure 11. HEK293 T cells viability by MTT assay for 48 h.

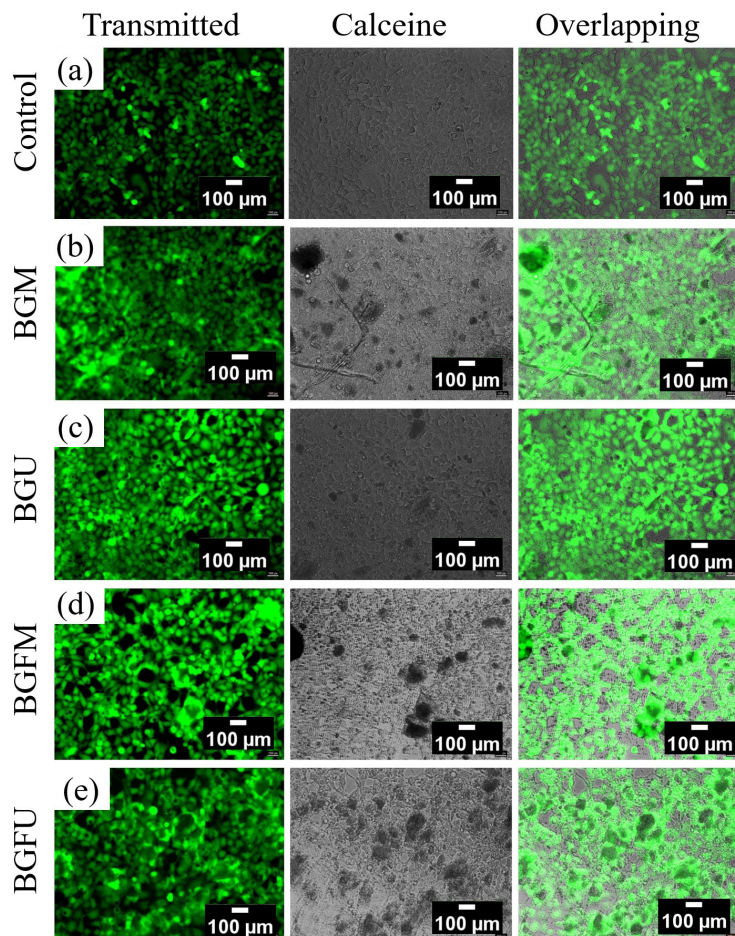


Figure 12. Green fluorescence (viable cells) and transmitted light images of HEK 293 T cells exposed to the direct contact of bioactive glass samples. (a) Control, (b) BGM, (c) BGU, (d) BGMF and (e) BGFU (Scale bar = 100px).

from the assays employed that the synthesized materials are potentially usable as biomaterials, since they did not present cytotoxicity to the cells of human embryonic kidney (HEK 293 T).

#### 4. Conclusion

Bioactive glass and Fluorine-containing bioactive glass synthesized by sol-gel route through mechanical stirring and ultrasound energy were successfully investigated in this work. Ultrasound energy and mechanical stirring applied to the sol-gel processing route make it possible to obtain spherical and dispersed particles with particle size between 197 nm–390 nm. The MET analyses showed that mechanical mixing is able to produce BG mesoporous structured, while BG produced by ultrasound energy had a dense bulk. The ability to form apatite in SBF medium was verified, and all samples are able to present a layer of HAC after 14 days in contact with physiological environment. The bioactive glass particles showed non-cytotoxic to HEK 293 T after 24 h MTT and Calcein assay. All these conditions favor that the materials developed in this study can be used as biomaterials. The results showed that there is an influence of the agitation method on the textural characteristics of the particles. In the sol-gel methodology employed in this study, by using ultrasonic energy for BG and BGF synthesis it was possible to identify largest surface areas for Fluorine-containing BG, in contrast to the non-fluorine-containing BG. One of the main purposes of producing BG by sol-gel route is to obtain a porous structure, which was not apparent for BGU particles. Therefore, the ultrasonic energy methodology would be disadvantageous for producing mesoporous particles from the route applied here. This study showed that mechanical agitation was more efficient to produce mesoporous particles to be applied as carrier of drugs and molecules to the biological environment, so BGM can be used as a more efficient biomaterial for such applications.

#### 5. Acknowledgments

The authors express their gratitude to Prof. Herman S. Mansur from the Center of Nanoscience, Nanotechnology and Innovation—CeNano2I/CEMUCASI/ UFMG for the DLS and FTIR analysis, as well as Prof. Dr. Maria de Fátima Leite of the Department of Physiology and Biophysics, UFMG for the *in vitro* analysis. The authors also gratefully acknowledge financial support from CNPq, CAPES and FAPEMIG/Brazil.

#### 6. References

- Jones JR. Reprint of: review of bioactive glass: from hench to hybrids. *Acta Biomater.* 2015;23:S53-82. <http://dx.doi.org/10.1016/j.actbio.2015.07.019>.
- Lins CEC, Oliveira AAR, Gonzalez I, Macedo WAA, Pereira MM. Structural analysis of fluorine-containing bioactive glass nanoparticles synthesized by sol-gel route assisted by ultrasound energy. *J Biomed Mater Res B Appl Biomater.* 2018;106(1):360-6. <http://dx.doi.org/10.1002/jbm.b.33846>.
- Lusvardi G, Malavasi G, Menabue L, Aina V, Morterra C. Fluoride-containing bioactive glasses: surface reactivity in simulated body fluids solutions. *Acta Biomater.* 2009;5(9):3548-62. <http://dx.doi.org/10.1016/j.actbio.2009.06.009>.
- Rabiee SM, Nazparvar N, Azizian M, Vashaei D, Tayebi L. Effect of ion substitution on properties of bioactive glasses: a review. *Ceram Int.* 2015;41(6):7241-51. <http://dx.doi.org/10.1016/j.ceramint.2015.02.140>.
- Christie JK, de Leeuw NH. Effect of strontium inclusion on the bioactivity of phosphate-based glasses. *J Mater Sci.* 2017;52(15):9014-22. <http://dx.doi.org/10.1007/s10853-017-1155-x>.
- Maçon ALB, Lee S, Poologasundarampillai G, Kasuga T, Jones JR. Synthesis and dissolution behaviour of CaO/SrO-containing sol-gel-derived 58S glasses. *J Mater Sci.* 2017;52(15):8858-70. <http://dx.doi.org/10.1007/s10853-017-0869-0>.
- Brauer DS, Mneimne M, Hill RG. Fluoride-containing bioactive glasses: fluoride loss during melting and ion release in tris buffer solution. *J Non-Cryst Solids.* 2011;357(18):3328-33. <http://dx.doi.org/10.1016/j.jnoncrystsol.2011.05.031>.
- Abbasi Z, Bahrololoum ME, Shariat MH, Bagheri R. Bioactive glasses in dentistry: a review. *J. Glas. Dent Rev.* 2015;2(1):1.
- Pereira MM, Clark AE, Hench LL. Calcium phosphate formation on sol-gel-derived bioactive glasses *in vitro*. *J Biomed Mater Res.* 1994;28(6):693-8. <http://dx.doi.org/10.1002/jbm.820280606>.
- Lukowiak A, Lao J, Lacroix J, Nedelec JM. Bioactive glass nanoparticles obtained through sol-gel chemistry. *Chem Commun.* 2013;49(59):6620. <http://dx.doi.org/10.1039/c3cc00003f>.
- Jafarzadeh M, Rahman IA, Sipaut CS. Synthesis of silica nanoparticles by modified sol-gel process: the effect of mixing modes of the reactants and drying techniques. *J Sol-Gel Sci Technol.* 2009;50(3):328-36. <http://dx.doi.org/10.1007/s10971-009-1958-6>.
- Zheng K, Boccaccini AR. Sol-gel processing of bioactive glass nanoparticles: a review. *Adv Colloid Interface Sci.* 2017;249:363-73. <http://dx.doi.org/10.1016/j.cis.2017.03.008>.
- Côté AS, Cormack AN, Tilocca A. Reactive molecular dynamics: an effective tool for modelling the sol-gel synthesis of bioglasses. *J Mater Sci.* 2017;52(15):9006-13. <http://dx.doi.org/10.1007/s10853-017-1009-6>.
- Hu Q, Li Y, Zhao N, Ning C, Chen X. Facile synthesis of hollow mesoporous bioactive glass sub-micron spheres with a tunable cavity size. *Mater Lett.* 2014;134:130-3. <http://dx.doi.org/10.1016/j.matlet.2014.07.041>.
- Pereira MM, Clark AE, Hench LL. Effect of texture on the rate of hydroxyapatite formation on gel-silica surface. *J Am Ceram Soc.* 1995;78(9):2463-8. <http://dx.doi.org/10.1111/j.1151-2916.1995.tb08686.x>.
- Oliveira AAR, Carvalho BB, Sander Mansur H, Magalhães Pereira M. Synthesis and characterization of bioactive glass particles using an ultrasound-assisted sol-gel process: engineering the morphology and size of sonogels via a poly(ethylene glycol) dispersing agent. *Mater Lett.* 2014;133:44-8. <http://dx.doi.org/10.1016/j.matlet.2014.06.092>.
- Rahman IA, Padavettan V. Synthesis of Silica nanoparticles by Sol-Gel: size-dependent properties, surface modification, and applications in silica-polymer nanocomposites: a review. *J Nanomater.* 2012;2012:1-15. <http://dx.doi.org/10.1155/2012/132424>.
- Zheng K, Taccardi N, Beltrán AM, Sui B, Zhou T, Marthala VRR, et al. Timing of calcium nitrate addition affects morphology, dispersity and composition of bioactive glass nanoparticles. *RSC Advances.* 2016;6(97):95101-11. <http://dx.doi.org/10.1039/C6RA05548F>.
- Utech S, Boccaccini AR. A review of hydrogel-based composites for biomedical applications: enhancement of hydrogel properties by addition of rigid inorganic fillers. New York: Springer; 2016.
- Kokubo T, Takadama H. How useful is SBF in predicting *in vivo* bone bioactivity? *Biomaterials.* 2006;27(15):2907-15. <http://dx.doi.org/10.1016/j.biomaterials.2006.01.017>.

21. Barrioni BR, Oliveira AC, Leite MF, Magalhães Pereira M. Sol-gel-derived manganese-releasing bioactive glass as a therapeutic approach for bone tissue engineering. *J Mater Sci*. 2017;52(15):8904-27. <http://dx.doi.org/10.1007/s10853-017-0944-6>.
22. Levy S, Van Dalen M, Agonafer S, Soboyejo WO. Cell/surface interactions and adhesion on bioactive glass 45S5. *J Mater Sci Mater Med*. 2007;18(1):89-102. <http://dx.doi.org/10.1007/s10856-006-0666-9>.
23. Moreira CDF, Carvalho SM, Sousa RG, Mansur HS, Pereira MM. Nanostructured chitosan/gelatin/bioactive glass in situ forming hydrogel composites as a potential injectable matrix for bone tissue engineering. *Mater Chem Phys*. 2018;218:304-16. <http://dx.doi.org/10.1016/j.matchemphys.2018.07.039>.
24. Ghadiri S, Hassanzadeh-Tabrizi SA, Bigham A. The effect of synthesis medium on structure and drug delivery behavior of CTAB-assisted sol-gel derived nanoporous calcium-magnesium-silicate. *J Sol-Gel Sci Technol*. 2017;83(1):229-36. <http://dx.doi.org/10.1007/s10971-017-4404-1>.
25. Rahman IA, Vejayakumaran P, Sipaut CS, Ismail J, Bakar MA, Adnan R, et al. An optimized sol-gel synthesis of stable primary equivalent silica particles. *Colloids Surf A Physicochem Eng Asp*. 2007;294(1-3):102-10. <http://dx.doi.org/10.1016/j.colsurfa.2006.08.001>.
26. Oliveira AAR, Souza DA, Dias LLS, Carvalho SM, Mansur HS, Magalhães Pereira M. Synthesis, characterization and cytocompatibility of spherical bioactive glass nanoparticles for potential hard tissue engineering applications. *Biomed Mater*. 2013;8(2):025011. <http://dx.doi.org/10.1088/1748-6041/8/2/025011>.
27. Lins CEC, Carvalho SM, Oliveira AAR, Magalhães Pereira M. Application of fluorine containing bioactive glass nanoparticles in dentin hypersensitivity treatment. *Key Eng Mater*. 2016;696(1):103-7. <http://dx.doi.org/10.4028/www.scientific.net/KEM.696.103>.
28. Pedone A, Charpentier T, Menziani MC. The structure of fluoride-containing bioactive glasses: new insights from first-principles calculations and solid state NMR spectroscopy. *J Mater Chem*. 2012;22(25):12599. <http://dx.doi.org/10.1039/c2jm30890h>.
29. Döhler F, Groh D, Chiba S, Bierlich J, Kobelke J, Brauer DS. Bioactive glasses with improved processing. Part 2. Viscosity and fibre drawing. *J Non-Cryst Solids*. 2016;432:130-6. <http://dx.doi.org/10.1016/j.jnoncrysol.2015.03.009>.
30. Lee JH, Kang MS, Mahapatra C, Kim HW. Effect of aminated mesoporous bioactive glass nanoparticles on the differentiation of dental pulp stem cells. *PLoS One*. 2016;11(3):1. <http://dx.doi.org/10.1371/journal.pone.0150727>.
31. Pereira MM, Hench LL. Mechanisms of hydroxyapatite formation on porous gel-silica substrates. *J Sol-Gel Sci Technol*. 1996;7(1-2):59-68. <http://dx.doi.org/10.1007/BF00401884>.
32. Melchers S, Uesbeck T, Winter O, Eckert H, Eder D. Effect of aluminum ion incorporation on the bioactivity and structure in mesoporous bioactive glasses. *Chem Mater*. 2016;28(10):3254-64. <http://dx.doi.org/10.1021/acs.chemmater.5b04117>.
33. Allothman ZA. A review: fundamental aspects of silicate mesoporous materials. *Materials*. 2012;5(12):2874-902. <http://dx.doi.org/10.3390/ma5122874>.
34. Thommes M. Physical adsorption characterization of nanoporous materials. *Chemieingenieurtechnik*. 2010;82(7):1059-73. <http://dx.doi.org/10.1002/cite.201000064>.
35. Barrioni BR, Norris E, Li S, Naruphontjirakul P, Jones JR, Pereira MM. Osteogenic potential of sol-gel bioactive glasses containing manganese. *J Mater Sci Mater Med*. 2019;30(7):86. <http://dx.doi.org/10.1007/s10856-019-6288-9>.
36. Shah FA. Fluoride-containing bioactive glasses: glass design, structure, bioactivity, cellular interactions, and recent developments. *Mater Sci Eng C*. 2016;58:1279-89. <http://dx.doi.org/10.1016/j.msec.2015.08.064>.
37. Wang Y, Pan H, Chen X. The preparation of hollow mesoporous bioglass nanoparticles with excellent drug delivery capacity for bone tissue regeneration. *Front Chem*. 2019;7:1. <http://dx.doi.org/10.3389/fchem.2019.00283>.
38. De Caluwé T, Vercryse CWJ, Declercq HA, Schaubroeck D, Verbeeck RMH, Martens LC. Bioactivity and biocompatibility of two fluoride containing bioactive glasses for dental applications. *Dent Mater*. 2016;32(11):1414-28. <http://dx.doi.org/10.1016/j.dental.2016.09.014>.
39. Pappas GS, Liatsi P, Kartsonakis IA, Danilidis I, Kordas G. Synthesis and characterization of new SiO<sub>2</sub>-CaO hollow nanospheres by sol-gel method: bioactivity of the new system. *J Non-Cryst Solids*. 2008;354(2-9):755-60. <http://dx.doi.org/10.1016/j.jnoncrysol.2007.09.007>.
40. Shah FA, Brauer DS, Hill RG, Hing KA. Apatite formation of bioactive glasses is enhanced by low additions of fluoride but delayed in the presence of serum proteins. *Mater Lett*. 2015;153:143-7. <http://dx.doi.org/10.1016/j.matlet.2015.04.013>.
41. Groh D, Döhler F, Brauer DS. Bioactive glasses with improved processing. Part 1: thermal properties, ion release and apatite formation. *Acta Biomater*. 2014;10(10):4465-73. <http://dx.doi.org/10.1016/j.actbio.2014.05.019>.
42. Mozafari M, Moztarzadeh F, Rabiee M, Azami M, Maleknia S, Tahiri M, et al. Development of macroporous nanocomposite scaffolds of gelatin/bioactive glass prepared through layer solvent casting combined with lamination technique for bone tissue engineering. *Ceram Int*. 2010;36(8):2431-9. <http://dx.doi.org/10.1016/j.ceramint.2010.07.010>.
43. Sriranganathan D, Chen X, Hing KA, Kanwal N, Hill RG. The effect of the incorporation of fluoride into strontium containing bioactive glasses. *J Non-Cryst Solids*. 2017;457:25-30. <http://dx.doi.org/10.1016/j.jnoncrysol.2016.11.018>.
44. Cocchi M, Durante C, Lusvardi G, Malavasi G, Menabue L. Evaluation of the behaviour of fluorine-containing bioactive glasses: reactivity in a simulated body fluid solution assisted by multivariate data analysis. *J Mater Sci Mater Med*. 2012;23(3):639-48. <http://dx.doi.org/10.1007/s10856-011-4543-9>.
45. Al-Noaman A, Rawlinson SCF, Hill RG. The influence of CaF<sub>2</sub> content on the physical properties and apatite formation of bioactive glass coatings for dental implants. *J Non-Cryst Solids*. 2012;358(15):1850-8. <http://dx.doi.org/10.1016/j.jnoncrysol.2012.05.039>.
46. Brauer DS, Karpukhina N, O'Donnell MD, Law RV, Hill RG. Fluoride-containing bioactive glasses: effect of glass design and structure on degradation, pH and apatite formation in simulated body fluid. *Acta Biomater*. 2010;6(8):3275-82. <http://dx.doi.org/10.1016/j.actbio.2010.01.043>.
47. Shah FA, Brauer DS, Wilson RM, Hill RG, Hing KA. Influence of cell culture medium composition on in vitro dissolution behavior of a fluoride-containing bioactive glass. *J Biomed Mater Res A*. 2014;102(3):647-54. <http://dx.doi.org/10.1002/jbm.a.34724>.
48. Oréfice RL, Pereira MM, Mansur HS. Biomateriais: fundamentos e aplicações. 1. ed. Rio de Janeiro: Cultura Medica; 2006.
49. Glavinias H, Von Richter O, Vojnits K, Mehn D, Wilhelm I, Nagy T, et al. Calcein assay: a high-throughput method to assess P-gp inhibition. *Xenobiotica*. 2011;41(8):712-9. <http://dx.doi.org/10.3109/00498254.2011.587033>.
50. Martin-Piedra MA, Garzon I, Oliveira AC, Alfonso-Rodriguez CA, Carriel V, Scionti G, et al. Cell viability and proliferation capability of long-term human dental pulp stem cell cultures. *Cytotherapy*. 2014;16(2):266-77. <http://dx.doi.org/10.1016/j.jcyt.2013.10.016>.